



**HAL**  
open science

## Gas-solid fluidized bed simulations using the filtered approach: Validation against pilot-scale experiments

Wenchao Yu, Pascal Fede, Mahdi Yazdanpanah, Benjamin Amblard, Florian Euzenat, Olivier Simonin

### ► To cite this version:

Wenchao Yu, Pascal Fede, Mahdi Yazdanpanah, Benjamin Amblard, Florian Euzenat, et al.. Gas-solid fluidized bed simulations using the filtered approach: Validation against pilot-scale experiments. *Chemical Engineering Science*, 2020, 217, pp.115472. 10.1016/j.ces.2020.115472 . hal-02502908

**HAL Id: hal-02502908**

**<https://ifp.hal.science/hal-02502908v1>**

Submitted on 9 Mar 2020

**HAL** is a multi-disciplinary open access archive for the deposit and dissemination of scientific research documents, whether they are published or not. The documents may come from teaching and research institutions in France or abroad, or from public or private research centers.

L'archive ouverte pluridisciplinaire **HAL**, est destinée au dépôt et à la diffusion de documents scientifiques de niveau recherche, publiés ou non, émanant des établissements d'enseignement et de recherche français ou étrangers, des laboratoires publics ou privés.

## **Gas-solid fluidized bed simulations using the filtered approach: Validation against pilot-scale experiments**

Wenchao Yu<sup>1</sup>, Pascal Fede<sup>1\*</sup>, Mahdi Yazdanpanah<sup>2</sup>,  
Benjamin Amblard<sup>3</sup>, Florian Euzenat<sup>2</sup> & Olivier Simonin<sup>1</sup>

<sup>1</sup>Institut de Mécanique des Fluides de Toulouse (IMFT), CNRS, Université de Toulouse,  
FR-31400 Toulouse, France.

<sup>2</sup>Total, Research & Technology Gonfreville (TRTG), Harfleur, 76700, France

<sup>3</sup>IFP Energies nouvelles, BP3, Solaize, 69360, France

\*Corresponding author. Email: pascal.fede@imft.fr

**Keywords:** Fluidized bed; Subgrid scale drag; Euler-Euler approach; CFD.

The numerical simulations on the large-scale fluidized beds still remain challenging due to the computational limitation and experimental validation. In the present work, a CFD study of a large-scale fluidized bed is investigated using the NEPTUNE\_CFD code based on an Eulerian n-fluid modeling approach. A SubGrid Scale (SGS) drag model based on the filtered approach is used to take into account the effect of very small solid structures unresolved with the coarse mesh. The numerical results are compared with the experimental data carried out in a pilot-scale fluidized bed unit and provided by Particulate Solid Research Inc (PSRI). By applying the SGS drag model without any specific or empirical tuning, mesh-independent numerical results are obtained. The flow regimes inside the fluidized bed are well predicted for all the superficial gas velocities studied here. The bed density profiles and the solid entrainment fluxes are also in good agreement with the experimental measurement.

- The large-scale fluidized bed simulations are validated against PSRI experiments for different flow regimes from turbulent to fast fluidization.
- A SGS drag model based on the filtered approach is using without any specific or empirical tuning which shows certain universality.
- The gas-solid flows inside the fluidized bed with different gas velocities are characterized.
- The validation in this study is a critical step toward industrial-scale fluidized bed simulations.

# Gas-solid fluidized bed simulations using the filtered approach: Validation against pilot-scale experiments

Wenchao Yu<sup>a</sup>, Pascal Fede<sup>\*a</sup>, Mahdi Yazdanpanah<sup>b</sup>, Benjamin Amblard<sup>c</sup>,  
Florian Euzenat<sup>b</sup>, Olivier Simonin<sup>a</sup>

<sup>a</sup>*Institut de Mécanique des Fluides de Toulouse (IMFT), Université de Toulouse, CNRS,  
FR-31400 Toulouse, France*

<sup>b</sup>*Total, Research & Technology Gonfreville (TRTG), Harfleur, 76700, France*

<sup>c</sup>*IFP Energies nouvelles, BP3, Solaize, 69360, France*

---

## Abstract

The numerical simulations on the large-scale fluidized beds still remain challenging due to the computational limitation and experimental validation. In the present work, a CFD study of a large-scale fluidized bed is investigated using the NEPTUNE-CFD code based on an Eulerian n-fluid modeling approach. A SubGrid Scale (SGS) drag model based on the filtered approach is used to take into account the effect of very small solid structures unresolved with the coarse mesh. The numerical results are compared with the experimental data carried out in a pilot-scale fluidized bed unit and provided by Particulate Solid Research Inc (PSRI). By applying the SGS drag model without any specific or empirical tuning, mesh-independent numerical results are obtained. The flow regimes inside the fluidized bed are well predicted for all the superficial gas velocities studied here. The bed density profiles and the solid entrainment fluxes are also in good agreement with the experimental measurement.

*Keywords:* Fluidized bed, Subgrid scale drag, Euler-Euler approach, CFD.

---

## 1. Introduction

Thanks to the high efficiency of mixing, mass and heat transfer of the gas-solid fluidized beds, it has become an indispensable equipment in many in-

---

\*Corresponding author. E-mail address: pascal.fede@imft.fr

dustrial applications, such as the fluid catalytic cracking (FCC) process in the  
5 petroleum refineries (Amblard et al. [1]). In order to optimize its design and  
improve its performance, the gas-solid fluidized bed has been widely studied in  
recent years. With the rapid development of the computational resources, CFD  
simulations have been used as a very important tool for the large-scale fluidized  
bed investigation. However, it has some specific challenges mainly related to  
10 the computation limitation and validation of the results. Even with HPC per-  
formances, the computational resources are still unaffordable for predicting the  
very small solid structures in the industrial-scale configurations using sufficiently  
fine grid. Therefore representative simulations of gas-solid fluidized bed on a  
coarse-grid is becoming a topic of great interest and challenge.

15 Igci and Sundaresan [2] and Parmentier et al. [3] have reported that the  
simulations on the coarse-grid would result in a major overestimation of bed  
expansion or solid entrainment, which is related to the drag overestimation due  
to the effect of unresolved structures on the resolved flow. Various numeri-  
cal methods and approaches to investigate and solve this problem have been  
20 well summarized and detailed in these reviews (van der Hoef et al. [4], Wang  
[5], Schneiderbauer et al. [6], Fullmer and Hrenya [7]). According to Wang [5],  
the empirical correlation or scaling factor methods were developed in the begin-  
ning, but they are only suitable for specific operating conditions and are difficult  
to be extended to other configurations. By assuming the important effect of the  
25 heterogeneous structures in the form of particle clusters, Energy Minimization  
Multi-Scale (EMMS) approach (Li and Kwauk [8, 9]) was developed to calculate  
the structure-dependent drag coefficients, which was successful to predict the  
hydrodynamics of Geldart A particles in circulating fluidized bed (CFB) flows  
(Wang et al. [10]). However, as mentioned by Li et al. [11], although the integra-  
30 tion of EMMS and Eulerian approach has significantly improved the calculation  
accuracy, the prediction of cluster diameters remains an unsolved problem which  
limits the application of their model only to Geldart A particles (not suitable  
for B, C and D particles). Deriving from the spatial averaging of the kinetic  
theory based two fluid model equations, the SGS drag models are usually closed

35 by filtering the well-resolved Euler-Euler simulations (Igci et al. [12], Igci and Sundaresan [2], Parmentier et al. [3], Ozel et al. [13], Schneiderbauer [14]). The correction given by these SGS drag models depends strongly on the filter size  $\bar{\Delta}$ . This dependence is generally defined as  $\bar{\Delta}^2/(\bar{\Delta}^2 + C)$ , where  $C$  is a constant evaluated from the general information of the configurations, such as particle  
40 terminal settling velocity, particle relaxation time, acceleration of the gravity, bed hydraulic diameter etc., according to these studies (Igci et al. [12], Igci and Sundaresan [2], Parmentier et al. [3], Schneiderbauer [14]). But it is defined as a variable in the study of Ozel et al. [13] where  $C$  depends on the local flow properties: the filtered particle relaxation time and the magnitude of the filtered  
45 relative velocity between gas and solid. With the help of a dynamic adjustment procedure by applying a second filter (see in [Appendix B](#) and Parmentier et al. [3]), the SGS drag model of Ozel et al. [13] closed by the fine-grid simulations on the CFB flow can also well predict the hydrodynamics in a dense fluidized bed investigated in Parmentier et al. [3] without any specific or empirical tuning,  
50 which shows certain universality.

To further show its applicability on the large-scale configuration from turbulent fluidized bed to quasi circulating fluidized bed, in the present work, the SGS drag model of Ozel et al. [13] is chosen to use in the simulations performed with NEPTUNE\_CFD code which is based on an Eulerian n-fluid modeling approach and validated with the experiments that were carried out in a pilot-scale  
55 fluidized bed unit provided by PSRI. The experimental validation of this numerical study is a critical step toward full scale simulation of industrial fluidized bed units.

The paper is organized as follows: [Section 2](#) and [Section 3](#) give the details  
60 about the experimental setup and numerical simulations, respectively. The mesh study in the absence of the SGS drag model is shown in [Section 4](#). In [Section 5](#), the effect of the SGS drag model is highlighted. The validation with different superficial gas velocities is presented in [Section 6](#). Conclusions are drawn in [Section 7](#).

## 65 2. Description of PSRI experiments

A number of experiments were performed by PSRI to measure the bubble properties (size, void fraction, frequency and velocity), solid circulation rate and bed density profiles in a  $0.9m$  diameter fluidized bed with Geldart Group A powders. More details are given below.

70 Tests were conducted in a  $0.89m$  inner diameter,  $6.85m$  tall steel fluidized bed unit shown in Fig. 1 (left), which contains three parts. The outlet on the top of the bed is connected by two cyclones to return the solid back to the bed. In Fig. 1 (right), an inside view of the test unit is presented. Fig. 1 (middle) shows the air distributor that is located at  $0.82m$ . The dipleg of the second cyclone  
75 has a part inside the bed, this leads to an annular shape for the bed outlet. According to the experimental observation, more than 99% of the entrained solids are returned into the bed through the dipleg of the first cyclone.

The experiments are operated with compressed dry air at ambient temperature at different superficial gas velocities varied from  $0.3$  to  $0.85m/s$ . The  
80 density and viscosity of air are  $1.18kg/m^3$  and  $1.85 \times 10^{-5}Pa \cdot s$ , respectively. The median size  $d_{p50}$  for the polydispersed particle is  $78\mu m$  with a density  $\rho_p = 1490kg/m^3$ . The total mass of solid particles inside the bed is estimated to  $1815kg$ .

Two sets of experimental data are selected to validate our simulations. The  
85 first one is the vertical bed density profile along the height of the bed, which is measured using a set of pressure transmitters at the pressure ports located along the bed wall. The responses of these pressure transmitters were time averaged, normalized by the spacing between two ports ( $L$ ) and the gravity  $g$  to give a vertical and localized bed density ( $DP/gL$ ). The second one to be compared is  
90 the overall entrainment rate of solid particles from the bed. It was measured by closing a pneumatically operated butterfly valve located in the first stage cyclone dipleg for thirty seconds.

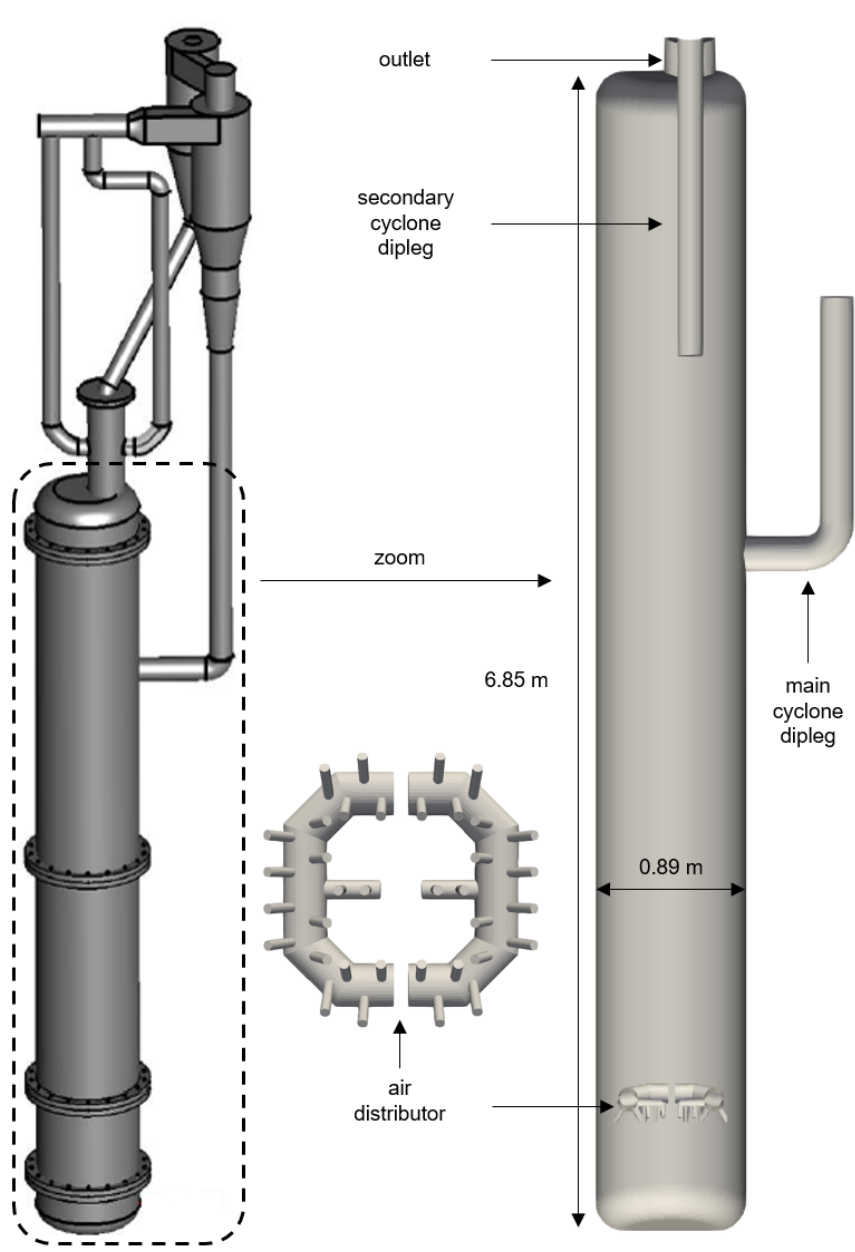


Figure 1: Geometry of 0.9m diameter fluidized bed of PSRI. Left: 3D model of the test unit, middle: air distributor and right: inside view of the test unit. Figures courtesy of PSRI.

### 3. Numerical simulation overview

The unsteady three dimensional numerical simulations of the fluidized-bed reactor were performed using the Eulerian N-fluid modeling approach for fluid-particle turbulent polydispersed reactive flows implemented in NEPTUNE\_CFD V4.0.1@Tlse version by IMFT (Institut de Mécanique des Fluides de Toulouse). NEPTUNE\_CFD is a computational multiphase flow software developed in the framework of the NEPTUNE project, financially supported by CEA (Commissariat à l'Énergie Atomique), EDF (Electricité de France), IRSN (Institut de Radioprotection et de Sûreté Nucléaire) and AREVA-NP. The approach is derived from a joint fluid-particle Probability Density Function (PDF) equation allowing to derive transport equations for the mass, momentum and agitation of particle phases. In the proposed modeling approach, transport equations (mass, momentum and fluctuating kinetic energy) are solved for each phase and coupled together through interphase transfer terms. For more details about the modeling approach and NEPTUNE\_CFD, readers are invited to see reference papers (Simonin [15], Gobin et al. [16], Fede et al. [17], Hamidouche et al. [18]).

The SGS drag model developed by Parmentier et al. [3] and Ozel et al. [13] is used to take into account the effect of the unresolved solid structures that cannot be solved on a coarse grid. The idea is similar to the filter approach using in the large eddy simulation in single-phase turbulent flow. A filter is applied to the transport equations. We assume that the filtered drag term can be split into a resolved part and an unresolved part. The unresolved part needs the model to close it using the resolved particle relaxation time and resolved particle and gas velocities. More details can be found in [Appendix A](#), Parmentier et al. [3] and Ozel et al. [13]. The model of Ozel et al. [13] is used and validated with the experimental results in this study.

[Fig. 2](#) shows the mesh on bed body, inside the bed and in the cross-section. Several simplifications have been made in order to use the structural mesh (hexahedral type). Compared to [Fig. 1](#) (right), the dipleg of the second cyclone is shifted horizontally to the center of bed. The dipleg of the first cyclone is



modeled by a square cross-sectional pipe. The nozzles of distributor are all neglected. The difference is less than 2% on the surface and volume after these  
 125 simplifications.

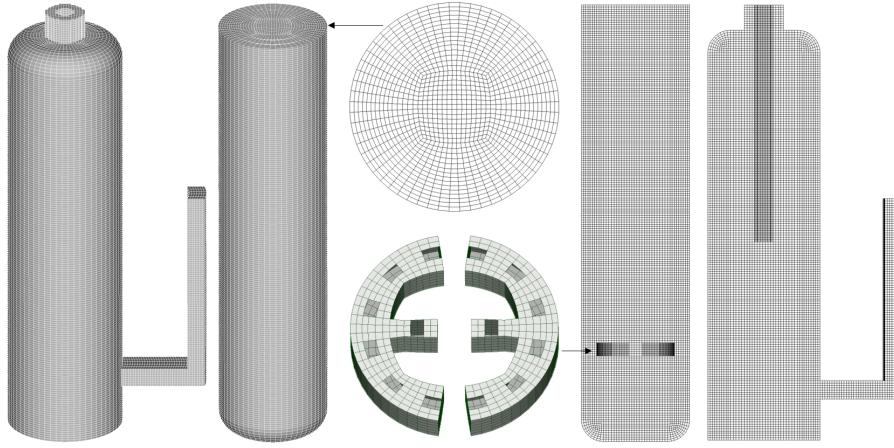


Figure 2: Mesh with 424,563 cells.

As the nozzles of air distributor are neglected in the mesh, the inlet air is set to directly blow to the bed bottom, in other words the gas flow rate is imposed normal to the cell. A free pressure condition is used at the outlet. The solid mass flow rate at the outlet is re-injected by the dipleg, the solid volume  
 130 fraction is imposed at 0.6. The internal dipleg is consider as dead-body. A friction wall boundary condition is used for the gas phase and a no-slip wall boundary condition is used for the solid phase. More details about the wall boundary condition of the solid phase can be found in Fede et al. [17].

Only the monodisperse cases are introduced here with  $d_p = d_{p50} = 78\mu m$ .  
 135 According to the large particle to gas density ratio, the drag force is dominant for mean gas-particle interphase momentum transfer. To take into account the effect of large solid volume fraction, the drag law of Gobin et al. [16] is selected here. For the gas phase we use  $k - \varepsilon$  model with additional terms that take into account the effect of particles on gas turbulence, and the turbulent viscosity  
 140 is also modified by the presence of solid phase. Particle agitation is modeled

by the approach of two transport equations  $q_p^2 - q_{gp}$ , one for particle agitation, and another for gas-particle covariance. Collisions between particles are also taken into account and assumed uncorrelated and inelastic, particle-particle restitution coefficient is set to 0.9. Due to the presence of high solid volume  
145 fraction in the actual study, the frictional interaction between solid particles becomes very important and it is considered by adding a frictional part in the solid stress tensor in the momentum equation (Bennani et al. [19]).

The numerical simulations are performed during 150s of physical time. Flow inside the fluidized bed is established around at 30s. It takes more time to  
150 achieve a balance on particle recycling through the cyclone dipleg with the increase of the superficial gas velocity. For the case  $V_f = 0.85m/s$ , the solid surface in the cyclone dipleg maintains in a certain level from 60s. Then, the time-averaged statistics are computed from 60s to the end of simulations (150s).

#### 4. Influence of mesh size

The influence of mesh size on the macroscopic behavior in the numerical  
155 simulations of fluidized beds has already been investigated (Agrawal et al. [20], Igci et al. [12], Parmentier et al. [3], Ozel et al. [13]). It is also closely investigated in this study regarding its vital role in industrial modeling where mesh size tends to be large due to scale effect. The SGS drag model mentioned in the section  
160 3 was developed to be able to reduce the impact of mesh size and can help to accurately predict the mean properties in the fluidized beds. In order to demonstrate the need to use the SGS drag model in this study, three meshes are generated and some details of these meshes are given in the Table 1. The SGS drag model is considered as not necessary if a mesh-independent result can  
165 be achieved within the reasonable computational cost for an industrial use.

Results of the simulations on different mesh sizes without the SGS drag model are presented here with the superficial gas velocity  $V_f = 0.6m/s$ . Fig. 3 shows the instantaneous solid volume fraction on the central plane. As the increase in the number of cells, a better resolution is obtained and finer structures

Number of cells	Typical cell size $L_{mesh}$ (mm)	$\frac{L_{mesh}}{d_p}$
91,613	30 ~ 40	385
424,563	18 ~ 25	231
1,737,736	11 ~ 16	141

Table 1: Some details of meshes used in this study.

170 can be observed. However, solid particles are still blown to all over the fluidized bed due to the overestimation of the drag force and nearly homogeneous particle distribution is formed for all the three meshes used here. Due to the too large solid circulating rate, a jet is formed at the dipleg of the main cyclone and hits directly the opposite wall.

175 Quantitatively, the mean vertical bed density profiles are compared to the experimental measurements in Fig. 4. The bed density was calculated from pressure drops measured along the height of the bed wall. From the experimental data, we know that the bed was separated into two regions, a dense region with a bed density close to  $700kg/m^3$  and a dilute region (free board) with very low solid concentration. It is clearly failed to be captured by the numerical results  
180 obtained with these meshes, a circulating bed is predicted and the jump at 3m above the air distributor corresponds to the jet returned by the dipleg.

The solid mass flow rates at the bed outlet are presented in Fig. 5. Corresponding to previous analysis, the solid fluxes oscillate between 100 and  $500kg/s$ .  
185 By reducing mesh size, a slight decrease of the time-averaged solid mass flow rate is observed, but it is still extremely higher than the experimental measurement which is  $0.77kg/s$  with  $V_f = 0.6m/s$ . Through these simulations, even with the finest mesh used here (1,737,736 cells), numerical results are still away from the experimental data, which suggests to refine again the mesh size. According  
190 to Andrews et al. [21], a mesh-independent solution could be obtained using a mesh size less than 10 particle diameters, which corresponds to around 5 billions cells for the actual cases. It exceeds the reasonable computational cost for

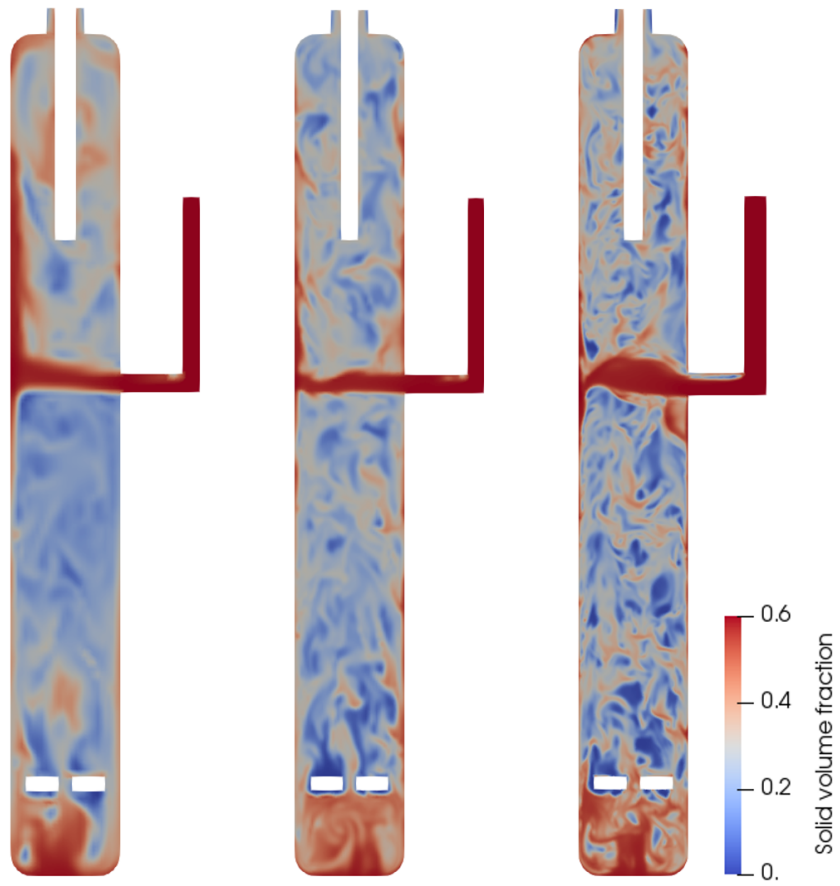


Figure 3: Instantaneous solid volume fraction on different mesh sizes without the SGS drag model. Left: 91,613 cells, middle: 424,563 cells and right: 1,737,736 cells.

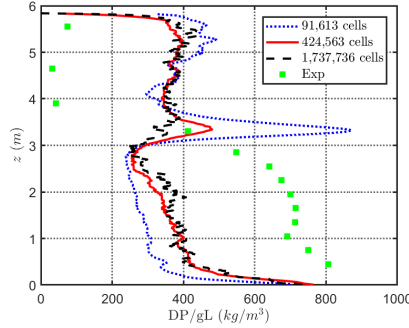


Figure 4: Profiles of mean vertical bed density on different mesh sizes without the SGS drag model.

a lab-scale gas-solid fluidized bed simulation. This issue is even more critical in case of industrial scale simulations where the bed size is more than 1 order of magnitude bigger than the pilot plant used in this study. Therefore, the SGS drag model is needed to overcome this problem.

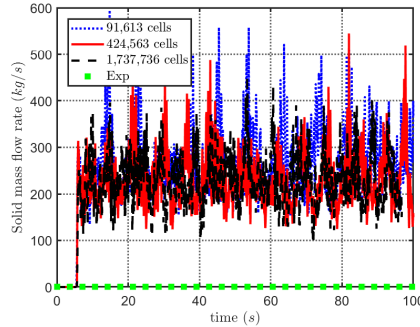


Figure 5: Comparison of experimental and predicted solid mass flow rate at the outlet versus time (s) on different mesh sizes without the SGS drag model.

## 5. Effect of the SGS drag model

The simulations with  $V_f = 0.6m/s$  are re-performed on three different mesh sizes in the presence of the SGS drag model. Fig. 6 shows the instantaneous solid volume fraction. The effect of the SGS drag model is obviously observed,

particle distributions are no longer homogeneous in the whole domain for the simulations on all the three meshes. A dense region is formed in the lower half of the fluidized bed while a dilute region is observed in the upper half. Meanwhile, less particles are entrained to the top region of the bed so that the solid mass flow rate decreases also at the bed outlet. More importantly, although the finer structures are resolved with the decrease of the mesh size, almost the same bed expansions are achieved for these three cases. It seems that a mesh-independent result is obtained in the presence of the SGS drag model.

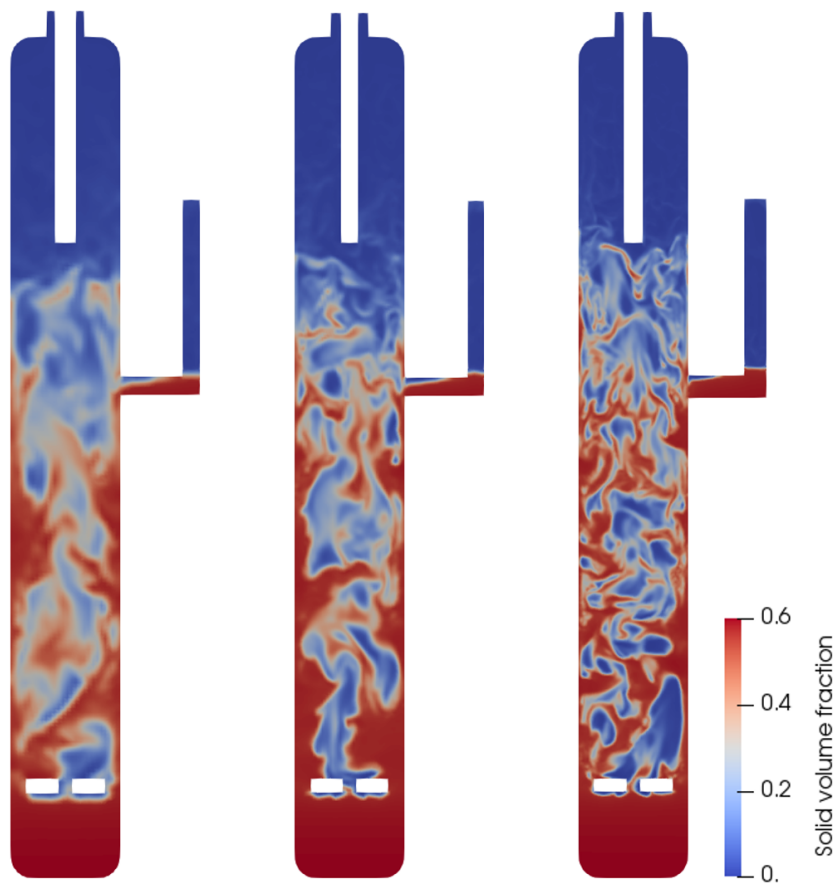


Figure 6: Instantaneous solid volume fraction for different mesh sizes with the SGS drag model. Left: 91,613 cells, middle: 424,563 cells and right: 1,737,736 cells.

These observations are confirmed quantitatively by Fig. 7 and Fig. 8. Compared to the cases without the SGS drag model, the mean vertical bed density profiles in Fig. 7 are much more improved and fit now to the experimental results. Meanwhile, the solid mass flow rates at the bed outlet decrease dramatically to the range between 0.4 to 1.3kg/s, very close to experimental measurement 0.77kg/s. Moreover, results between different mesh sizes are similar to each other. This indicates that the SGS drag model developed in Ozel et al. [13] achieves to do a larger drag correction in the case with larger mesh size and to do a smaller drag correction with finer mesh size without any specific or empirical tuning.

In terms of the computational resources consumption for these three cases, it takes around 24,400 CPU hours for the case with mesh 1,737,736 cells for running 150 seconds physical time, that corresponds roughly to 3 days of computational time on 360 cores, while it takes only 3,430 CPU hours for the mesh 424,563 cells and 140 CPU hours for the mesh 91,613 cells. Thus, the mesh with 424,563 cells has been selected for the following studies as a good compromise on the flow resolution and computational cost.

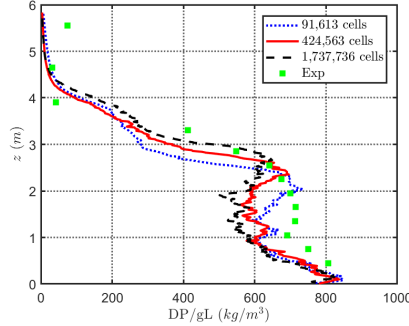


Figure 7: Profiles of mean vertical bed density for different mesh sizes with the SGS drag model.

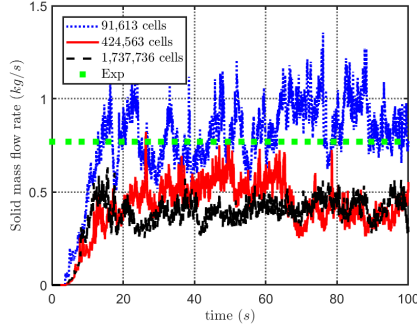


Figure 8: Solid mass flow rate at the outlet versus time (s) for different mesh sizes with the SGS drag model.

## 6. Superficial gas velocities

### 6.1. Validation

The simulations are performed for different superficial gas velocities  $V_f = 0.3, 0.6$  and  $0.85m/s$  in the presence of the SGS drag model. Fig. 9 shows the instantaneous solid volume fractions. Bed expansion is enhanced with the increase of superficial gas velocity. With  $V_f = 0.3m/s$ , a dense fluidized bed is obtained, particles rarely escape from the bed outlet. Increasing the superficial gas velocity to  $0.6m/s$ , as mentioned in the previous section, two regimes exist, one dense regime in the lower part and one dilute regime in the upper part. A small quantity of particles can fly up to the bed outlet and recycles through the main cyclone dipleg. Increasing again to  $V_f = 0.85m/s$ , the expanded bed height can reach the lower part of the secondary cyclone dipleg, a circulating fluidized bed is nearly formed, particles are going to fill the cyclone dipleg.

In Fig. 10 (left), a very similar trend is observed compared to experimental bed density profiles for three superficial gas velocities. Bed densities in dense region are underestimated for all three cases as shown in Fig. 10 (right), 11% for the case of  $V_f = 0.3m/s$ , 8% for  $V_f = 0.6m/s$  and 2% for  $V_f = 0.85m/s$ . It should be noted that the total mass of solid particles in the bed used in these simulations is only an estimation of mass computed from experimental density profiles. In addition, the bed holdup is a dynamic value which depends on the



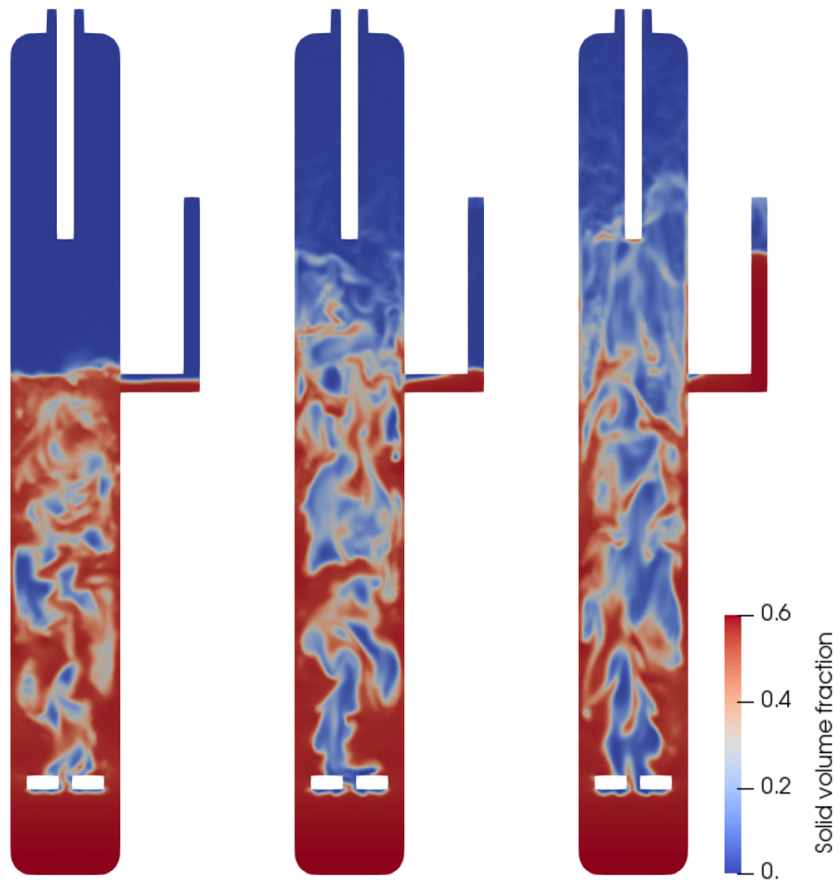


Figure 9: Instantaneous solid volume fraction for different gas velocities. Left:  $V_f = 0.3\text{ m/s}$ , middle:  $V_f = 0.6\text{ m/s}$  and right:  $V_f = 0.85\text{ m/s}$ .

operating conditions. Therefore obtaining precise value from experimental results is not possible. Considering the case of  $V_f = 0.3m/s$  as an example, the difference of  $87.5kg/m^3$  for the bed density between the numerical prediction and the experimental measurement in the dense region could make a difference of around  $140kg$  for particle mass estimation. Hence, one reason of the under-estimation of the bed density may come from the difference of the total solid mass used in the simulations and experiments.

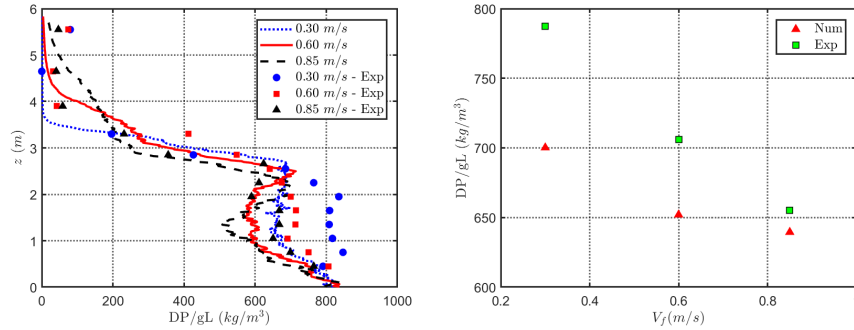


Figure 10: Left: Profiles of mean vertical bed density for different gas velocities and right: average bed density in the dense region for different gas velocities.

In Fig. 11, the solid mass flow rates at the bed outlet are presented and compared with experimental results. Considering the influences from the mass estimation problem mentioned in the previous paragraph and the monodisperse assumption, it is totally acceptable to have a predicted solid mass flow rate slightly underestimated but still rested in the same order of magnitude compared to the experimental result for the case  $V_f = 0.6m/s$ . More importantly, an exponential augmentation of the solid mass flow rate is well captured when increasing superficial gas velocities. From  $V_f = 0.3$  to  $0.85m/s$ , the flow regime changes from a turbulent fluidized bed to a quasi circulating fluidized bed, the recirculation rate is amplified by several orders of magnitude, from  $10^{-3}$  to  $10^0kg/s$ .

After these validations, some more details about results are given below.

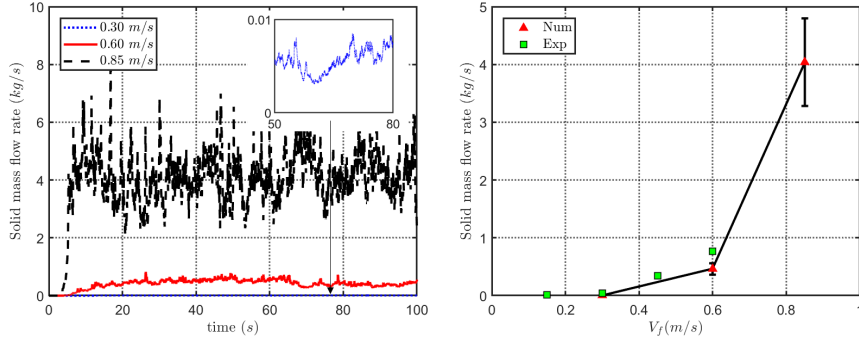


Figure 11: Left: Solid mass flow rate at the outlet versus time (s) for different gas velocities and right: time-averaged solid mass flow rate compared to experimental data.

## 265 6.2. Solid volume fraction

The mean solid volume fractions for different gas velocities are shown in Fig. 12. For all the three cases, high solid volume fraction is found in the near wall region and low solid volume fraction at the bed center. And it is obvious to see that there are two peaks of the solid volume fraction close to the wall, one is just above the air distributor, corresponding to the large number of particles blown up by the air, another one is located below the main cyclone dipleg, corresponding to particles going down by the gravity and by the return of the dipleg.

Fig. 13 shows the radial profiles of time- and spatial-averaged solid volume fraction for different gas velocities at four horizontal planes. Generally, for the first three planes below the main cyclone dipleg ( $z = 0.7, 1.7$  and  $2.7m$ ), the profiles have a minimum at the center of the bed and a maximum at the wall for all the three cases. At the plane above the main cyclone dipleg  $z = 3.7m$ , where is the transition zone between the dense region and the dilute region, the minimum is found not at the bed center but at  $r/R \sim 0.75$ , except the case  $V_f = 0.3m/s$  where rare particles can reach this height. Moreover, mean solid volume fraction decreases with the increase of the superficial gas velocity all along the radial direction at the first three planes.

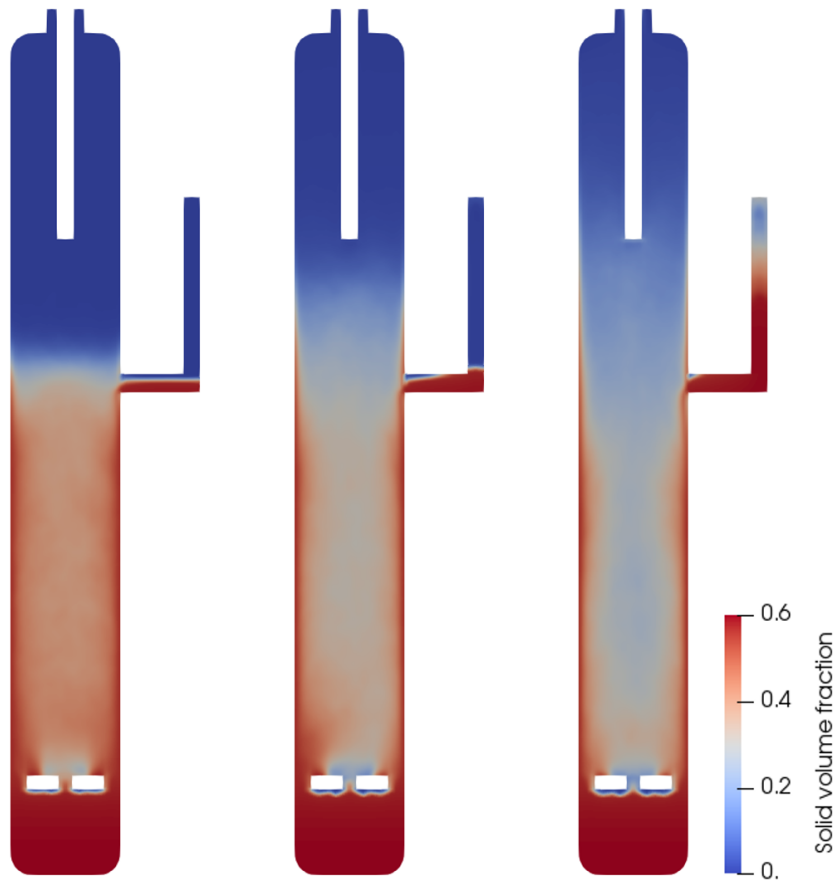


Figure 12: Mean solid volume fraction for different gas velocities. Left:  $V_f = 0.3m/s$ , middle:  $V_f = 0.6m/s$  and right:  $V_f = 0.85m/s$ .

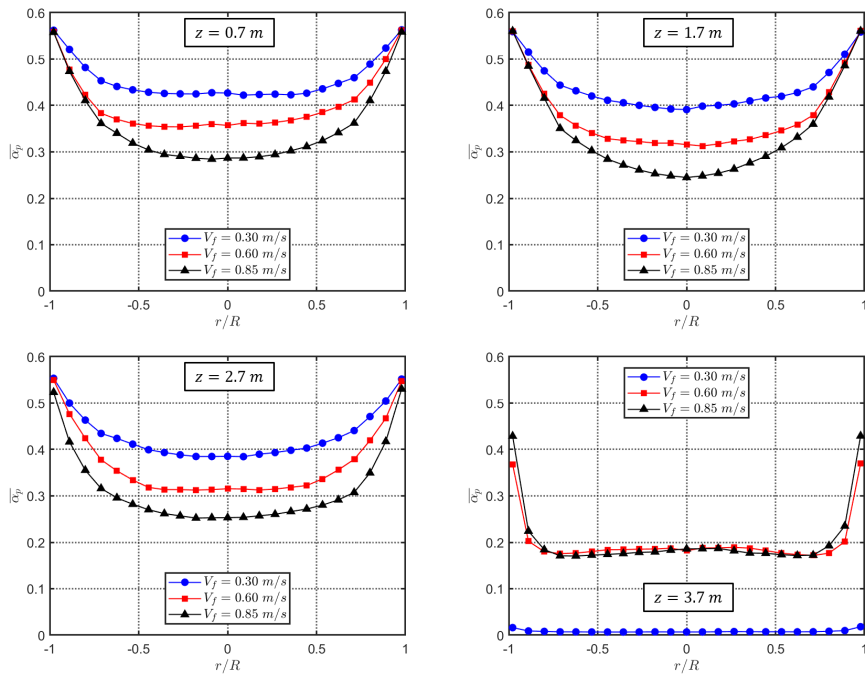


Figure 13: Radial profiles of time- and spatial-averaged solid volume fraction for different gas velocities at four horizontal planes. Upper-left:  $z = 0.7\text{ m}$ , upper-right:  $z = 1.7\text{ m}$ , lower-left:  $z = 2.7\text{ m}$  and lower-right:  $z = 3.7\text{ m}$ .

### 6.3. Solid velocity

285 **Fig. 14** shows the time- and spatial-averaged solid velocity field from the top of the air distributor to the bottom of the secondary cyclone dipleg for different gas velocities. The radial axis is amplified twice in order to see more clearly the velocity vectors. In general, particles move upwards at the center of the bed and downwards in the near wall region, and only one single clockwise macroscopic  
 290 mixing loop is formed for all three gas velocities.

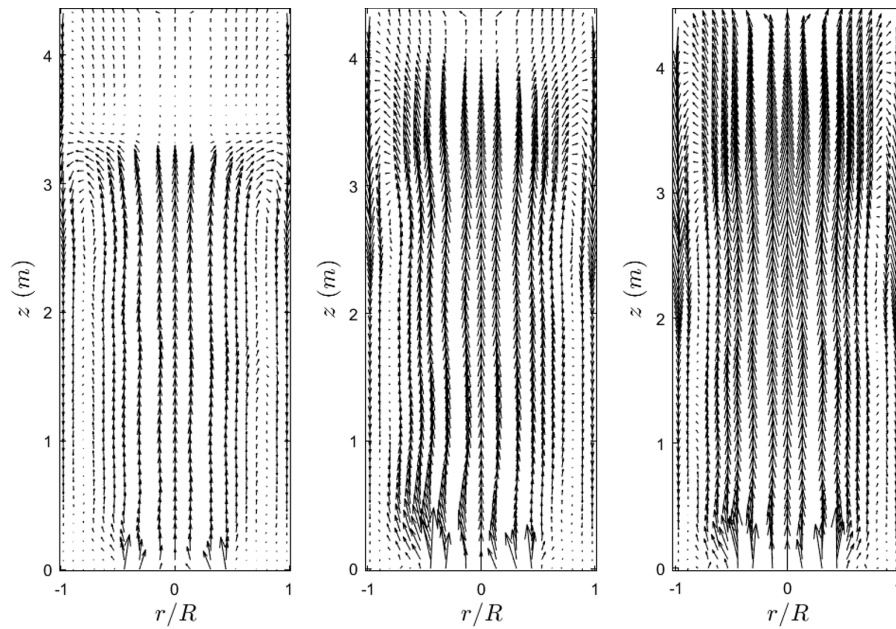


Figure 14: Time- and spatial-averaged solid velocity field from the top of the air distributor to the bottom of the secondary cyclone dipleg for different gas velocities. Left:  $V_f = 0.3m/s$ , middle:  $V_f = 0.6m/s$  and right:  $V_f = 0.85m/s$ .

The radial profiles of the time- and spatial-averaged solid vertical velocity normalized by the superficial gas velocity are presented in **Fig. 15**. The profiles have a positive peak at the center of the bed and a negative minimum at the wall. From  $z = 0.7$  to  $2.7m$ , particles move faster upwards at the bed center and downwards at the wall for all the three cases. At  $z = 3.7m$ , particles are  
 295 slowing down due to the effect of the gravity.

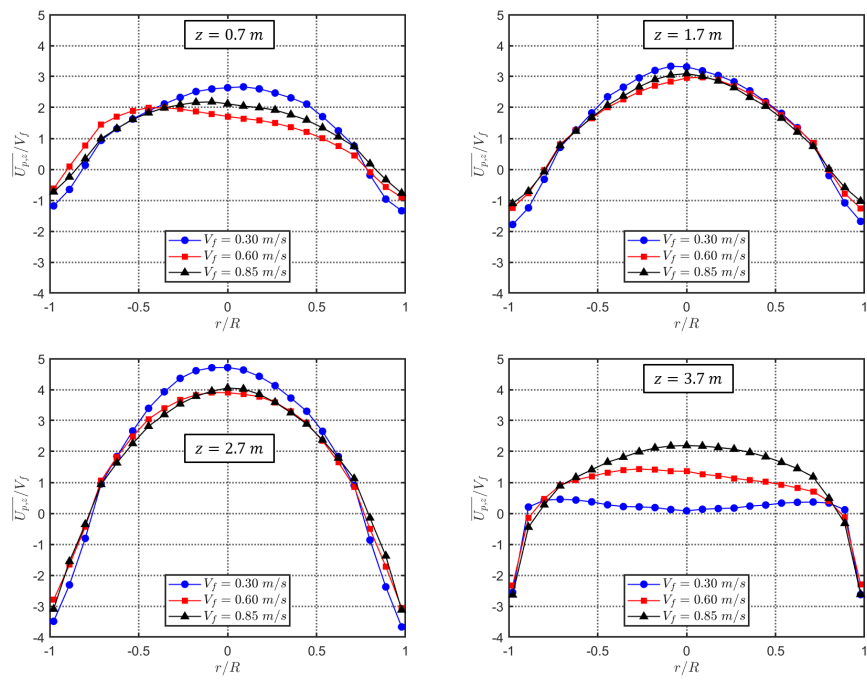


Figure 15: Radial profiles of time- and spatial-averaged solid vertical velocity for different gas velocities at four horizontal planes. Upper-left:  $z = 0.7\text{ m}$ , upper-right:  $z = 1.7\text{ m}$ , lower-left:  $z = 2.7\text{ m}$  and lower-right:  $z = 3.7\text{ m}$ .

#### 6.4. Solid mass flow rate

The mean solid mass flow rates normalized by the inlet gas mass flow rate at different horizontal planes are presented in Fig. 16. It can be clearly observed that solid particle flux goes upward through the bed center and goes downwards along the bed wall for all the three cases. The strongest gradient of the solid mass flow rate in the plane is found for the case  $V_f = 0.3\text{m/s}$ , that corresponds to a dense fluidized bed for mixing, while the weakest gradient is found for the case  $V_f = 0.85\text{m/s}$  corresponding to a circulating fluidized bed for particle transport.

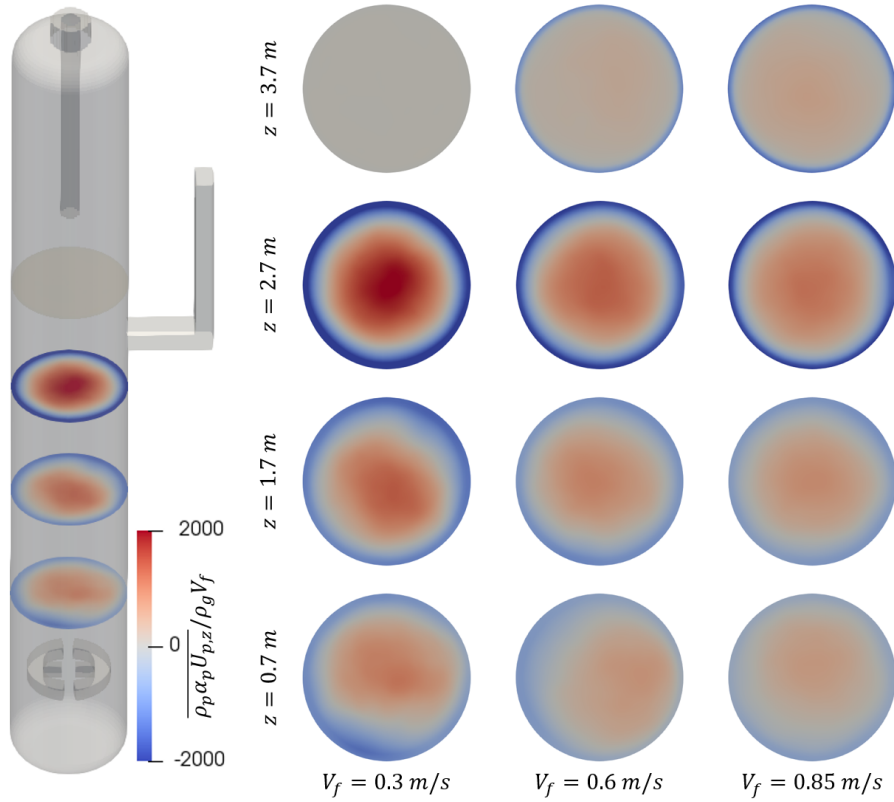


Figure 16: Mean solid mass flow rate for different gas velocities at four horizontal planes along the bed height. Left:  $V_f = 0.3\text{m/s}$ , middle:  $V_f = 0.6\text{m/s}$  and right:  $V_f = 0.85\text{m/s}$ .

Fig. 17 shows the radial profiles of time- and spatial-averaged solid mass



flow rate normalized by the inlet gas mass flow rate at four horizontal planes. The positive solid mass flow rate at the bed center increases with the bed height from  $z = 0.7$  to  $2.7m$ , decreases at the highest plane. The same description can  
 310 be used for the negative solid mass flow rate at the wall.

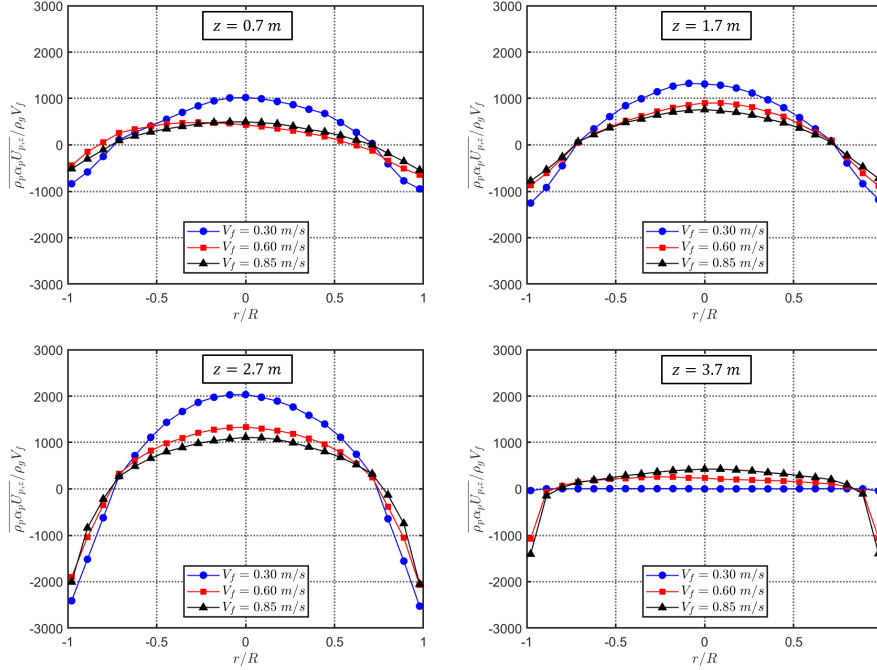


Figure 17: Radial profiles of time- and spatial-averaged solid mass flow rate for different gas velocities at four horizontal planes. Upper-left:  $z = 0.7m$ , upper-right:  $z = 1.7m$ , lower-left:  $z = 2.7m$  and lower-right:  $z = 3.7m$ .

## 7. Conclusion

A CFD study of a large-scale fluidized bed is investigated using the NEPTUNE\_CFD code based on an Eulerian n-fluid modeling approach. A major overestimation of the bed expansion is observed for the simulations on the coarse  
 315 meshes which shows the necessity of using a SGS drag model. With the application of the SGS drag model developed by Ozel et al. [13] without any specific or empirical tuning, the mesh-independent numerical results are obtained. The

flow regimes inside the fluidized bed are well predicted for three different superficial gas velocities. The bed density profiles and the solid entrainment fluxes are also in good agreement with the experimental measurement. The validation  
 320 of these simulations enhances the credibility of using such a SGS drag model and provides a feasibility for the further numerical study on industrial-scale fluidized bed.

### Acknowledgments

This work was performed using HPC resources from CALMIP (Grant 2018  
 325 - p0111) and from CINES Occigen under the allocation  $n^\circ A0022B06012$  and  $n^\circ A0042B06012$ . The authors are grateful to S. Sundaram, A. Issangya, B. Freireich, R. Cocco and S.B. Reddy Karri from Particulate Solid Research Inc. for sharing their experimental data in the 0.9m diameter fluidized bed.

### 330 Appendix A. Derivation of filtered Euler-Euler two-phase model

In this appendix the set of the filtered equations of the multi-fluid Eulerian model is introduced. Hereafter, the gas phase corresponds to the subscript  $k = g$  and the particulate phase to  $k = p$ .

Let  $\alpha_k(\mathbf{x}, t)$  denote the volume fraction of phase  $k$  at location  $\mathbf{x}$  and time  $t$  obtained by solving the Euler-Euler two-phase model equations. We can define the filtered phase volume fraction as

$$\bar{\alpha}_k(\mathbf{x}, t) = \int \int \int \alpha_k(\mathbf{r}, t) G(\mathbf{r} - \mathbf{x}) d\mathbf{r} \quad (\text{A.1})$$

where  $G(\mathbf{r} - \mathbf{x})$  is a weight function that satisfies  $\int \int \int G(\mathbf{r}) d\mathbf{r} = 1$ . The filtered velocity of phase  $k$  is defined as

$$\tilde{U}_k(\mathbf{x}, t) = \frac{1}{\bar{\alpha}_k} \int \int \int \alpha_k(\mathbf{r}, t) G(\mathbf{r} - \mathbf{x}) U_k(\mathbf{r}, t) d\mathbf{r} \quad (\text{A.2})$$

Applying such a filter to the mass balance equation for the phase  $k$ , we obtain

$$\frac{\partial}{\partial t} \rho_k \bar{\alpha}_k + \frac{\partial}{\partial x_j} \rho_k \bar{\alpha}_k \tilde{U}_{k,j} = 0 \quad (\text{A.3})$$

This filtering procedure can be applied to momentum balance equation for the phase  $k$ , we have

$$\begin{aligned}
\frac{\partial}{\partial t} \rho_k \bar{\alpha}_k \tilde{U}_{k,j} + \frac{\partial}{\partial x_j} \rho_k \bar{\alpha}_k \tilde{U}_{k,i} \tilde{U}_{k,j} = & \rho_k \bar{\alpha}_k g_i \\
& - \bar{\alpha}_k \frac{\partial \bar{P}_g}{\partial x_i} - \varphi_{k,i}^{sgs} \\
& + \tilde{I}_{k,i} + I_{k,i}^{sgs} \\
& - \frac{\partial}{\partial x_j} \tilde{\Sigma}_{k,ij} - \frac{\partial}{\partial x_j} \Sigma_{k,ij}^{sgs} \\
& - \frac{\partial}{\partial x_j} \rho_k \bar{\alpha}_k \sigma_{k,ij}^{sgs}
\end{aligned} \tag{A.4}$$

Terms with superscript ( $sgs$ ) in Eq. (A.4) appear from the filtering process and they represent the interaction between resolved and subgrid contributions. The first term on the right is the gravity contribution. The second line is the resolved and subgrid buoyancy force. The third line shows the resolved and subgrid drag force. The fourth line is the resolved and subgrid stress tensor. The last terms is a Reynolds stress-like contribution coming from the fluctuation velocity of phase  $k$ . Thus, four subgrid terms have to be closed. According to the budget analysis in Parmentier et al. [3] and Ozel et al. [13], the subgrid drag force has a dominant effect on the prediction of the bed expansion. Therefore, in the actual study, we focus on the modeling of the subgrid drag force term  $I_{k,i}^{sgs}$  and choose to neglect three other contributions. The drag force terms  $\tilde{I}_{k,i}$  and  $I_{k,i}^{sgs}$  are defined as

$$\tilde{I}_{g,i} = -\tilde{I}_{p,i} = \frac{\rho_p \bar{\alpha}_p}{\tilde{\tau}_{gp}^F} (\tilde{U}_{p,i} - \tilde{U}_{g,i}) \tag{A.5}$$

$$I_{g,i}^{sgs} = -I_{p,i}^{sgs} = \frac{\overline{\rho_p \alpha_p}}{\tau_{gp}^F} V_{r,i} - \frac{\rho_p \bar{\alpha}_p}{\tilde{\tau}_{gp}^F} (\tilde{U}_{p,i} - \tilde{U}_{g,i}) \tag{A.6}$$

where  $V_{r,i} = U_{p,i} - U_{g,i}$  is the relative velocity,  $\tau_{gp}^F$  is the mean particle relaxation time. The filtered drag force can be approximated by

$$\frac{\overline{\rho_p \alpha_p}}{\tau_{gp}^F} V_{r,i} \simeq \frac{\rho_p}{\tilde{\tau}_{gp}^F} \overline{\alpha_p V_{r,i}} \tag{A.7}$$

where  $\overline{\alpha_p V_{r,i}} = \bar{\alpha}_p (\tilde{U}_{p,i} - \tilde{U}_{g@p,i})$ . By introducing a subgrid drift velocity  $\tilde{V}_{d,i}$  which is defined as the difference between the filtered gas velocity seen by the

particle phase and the filtered gas velocity seen by the gas phase,  $\tilde{V}_{d,i} = \tilde{U}_{g@p,i} - \tilde{U}_{g,i}$ , Eq. (A.6) becomes

$$I_{g,i}^{sgs} = -I_{p,i}^{sgs} = -\frac{\rho_p \bar{\alpha}_p}{\tilde{\tau}_{gp}^F} \tilde{V}_{d,i} \quad (\text{A.8})$$

According to Parmentier et al. [3],  $\tilde{V}_{d,i}$  can be modeled by:

$$\tilde{V}_{d,i} = -g(\bar{\Delta}, \bar{\alpha}_p) K_{ij} \left( \tilde{U}_{p,j} - \tilde{U}_{g,j} \right) \quad (\text{A.9})$$

where  $g(\bar{\Delta}, \bar{\alpha}_p)$  is a function of the filter size  $\bar{\Delta}$  and filtered particle volume fraction  $\bar{\alpha}_p$ , it can be approximated by a multiplication of two independent functions  $f(\bar{\Delta})$  and  $h(\bar{\alpha}_p)$ .  $K_{ij}$  is a second order symmetric tensor. It is assumed that  $K_{xy} = K_{yz} = K_{xz} = 0$  and  $K_{xx} = K_{yy}$  for the three-dimensional fluidized bed simulations where the gravity is in the  $z$ -direction. Thus,  $\tilde{V}_{d,i}$  can be evaluated by

$$\tilde{V}_{d,\beta} = -K_{\beta\beta} f(\bar{\Delta}) h(\bar{\alpha}_p) \left( \tilde{U}_{p,\beta} - \tilde{U}_{g,\beta} \right) \quad (\text{A.10})$$

where the Greek subscript  $\beta = x, y, z$  and is used to indicate that there is no implicit summation. The constant  $K_{\beta\beta}$  is dynamically adjusted by a procedure detailed in Appendix B.  $h(\bar{\alpha}_p)$  is measured from fine-grid simulations and given as

$$h(\bar{\alpha}_p) = -\tanh\left(\frac{\bar{\alpha}_p}{0.1}\right) \sqrt{\frac{\bar{\alpha}_p}{0.64}} \left(1 - \frac{\bar{\alpha}_p}{0.64}\right)^2 \left(1 - 1.88 \frac{\bar{\alpha}_p}{0.64} + 5.16 \left(\frac{\bar{\alpha}_p}{0.64}\right)^2\right) \quad (\text{A.11})$$

The following form is proposed for  $f(\bar{\Delta})$ ,

$$f(\bar{\Delta}) = \frac{\bar{\Delta}^2}{\bar{\Delta}^2 + C} \quad (\text{A.12})$$

where  $C = 0.15 \tilde{\tau}_{gp}^F |\tilde{V}_r|^2$ ,  $|\tilde{V}_r|$  is the magnitude of the filtered relative velocity. To summarize, the filtered drag force is modeled by:

$$\overline{\frac{\rho_p \bar{\alpha}_p}{\tau_{gp}^F} V_{r,\beta}} = \frac{\rho_p \bar{\alpha}_p}{\tilde{\tau}_{gp}^F} (1 + K_{\beta\beta} f(\bar{\Delta}) h(\bar{\alpha}_p)) \left( \tilde{U}_{p,\beta} - \tilde{U}_{g,\beta} \right) \quad (\text{A.13})$$

335 It should be noted that a clipping is applied to  $K_{\beta\beta} f(\bar{\Delta}) h(\bar{\alpha}_p)$  in these simulations in order to remove those values lower than -0.99999, avoiding a filtered drag force in the direction opposite to its resolved part.

## Appendix B. Dynamic adjustment of the model constant $K_{\beta\beta}$

Parmentier et al. [3] proposed adjusting the model constants  $K_{\beta\beta}$  dynamically by using a method adapted from Germano et al. [22] and Lilly [23]. The constant are dependent on both the case simulated and the direction. The idea is to estimate values of  $K_{\beta\beta}$  for each cell during the simulation on a coarse grid, by performing a filtering operation of variables over cells in the neighborhood. Test-level filtered function  $\hat{f}$  can be averaged over the base level function  $\bar{f}$  for a uniform 3D mesh

$$\begin{aligned} \hat{f}(\mathbf{x}, t) = & \frac{1}{7}(\bar{f}(\mathbf{x}, t) + \bar{f}(\mathbf{x} + \hat{\Delta}\mathbf{e}_x, t) + \bar{f}(\mathbf{x} - \hat{\Delta}\mathbf{e}_x, t) + \bar{f}(\mathbf{x} + \hat{\Delta}\mathbf{e}_y, t) \\ & + \bar{f}(\mathbf{x} - \hat{\Delta}\mathbf{e}_y, t) + \bar{f}(\mathbf{x} + \hat{\Delta}\mathbf{e}_z, t) + \bar{f}(\mathbf{x} - \hat{\Delta}\mathbf{e}_z, t)) \end{aligned} \quad (\text{B.1})$$

where  $\hat{\Delta}$  is the test-level filter width. Parmentier et al. [3] tested the function  $f(\bar{\Delta})$ ,  $g(\bar{\alpha}_p)$  at the test and the base filter levels. They state the both functions are nearly independent of the choice of the filter width. The model at the base level is given by:

$$\begin{aligned} \bar{\alpha}_p \tilde{V}_{d,\beta} = & -\overline{\alpha_p(U_{p,\beta} - U_{g,\beta})} + \bar{\alpha}_p(\tilde{U}_{p,\beta} - \tilde{U}_{g,\beta}) \\ = & -\bar{\alpha}_p K_{\beta\beta} f(\bar{\Delta}) h(\bar{\alpha}_p) (\tilde{U}_{p,\beta} - \tilde{U}_{g,\beta}) \end{aligned} \quad (\text{B.2})$$

Consequently, one can define the subgrid drift velocity  $\mathcal{T}_\beta$  at test scale obeying the same modeling assumption as

$$\begin{aligned} \mathcal{T}_\beta = & -\overline{\alpha_p(U_{p,\beta} - U_{g,\beta})} + \hat{\alpha}_p(\hat{U}_{p,\beta} - \hat{U}_{g,\beta}) \\ = & -\hat{\alpha}_p K_{\beta\beta} f(\hat{\Delta}) h(\hat{\alpha}_p) (\hat{U}_{p,\beta} - \hat{U}_{g,\beta}) \end{aligned} \quad (\text{B.3})$$

The filtered subgrid drift velocity is given by:

$$\mathcal{F}_\beta = \widehat{\bar{\alpha}_p \tilde{V}_{d,\beta}} = -\overline{\alpha_p(U_{p,\beta} - U_{g,\beta})} + \overline{\bar{\alpha}_p(\tilde{U}_{p,\beta} - \tilde{U}_{g,\beta})} \quad (\text{B.4})$$

The difference between the filtered subgrid drift velocity (Eq. (B.4)) and the subgrid drift velocity at the test scale (Eq. (B.3)) is

$$\mathcal{L}_\beta = \mathcal{F}_\beta - \mathcal{T}_\beta = \overline{\bar{\alpha}_p(\tilde{U}_{p,\beta} - \tilde{U}_{g,\beta})} - \hat{\alpha}_p(\hat{U}_{p,\beta} - \hat{U}_{g,\beta}) \quad (\text{B.5})$$

Moreover, assuming that the variation of  $K_{\beta\beta}$  is negligible between two different scale levels, substitution of Eq. (B.2) and Eq. (B.3) into Eq. (B.5) leads to the following relations:

$$\mathcal{L}_\beta = -K_{\beta\beta}\mathcal{M}_\beta \quad (\text{B.6})$$

where  $\mathcal{M}_\beta = \overline{f(\widehat{\Delta})h(\widehat{\alpha}_p)\widehat{\alpha}_p(\widetilde{U}_{p,\beta} - \widetilde{U}_{g,\beta})} - f(\widehat{\Delta})h(\widehat{\alpha}_p)\widehat{\alpha}_p(\widehat{U}_{p,\beta} - \widehat{U}_{g,\beta})$ . Thus, we can obtain a model coefficient as

$$K_{\beta\beta} \approx -\frac{\mathcal{L}_\beta}{\mathcal{M}_\beta} \quad (\text{B.7})$$

For three-dimensional simulations, the model coefficients along  $x$ - and  $y$ -directions are assumed to be the same and given by following relation:

$$K_{xx} = K_{yy} = -\frac{\mathcal{L}_x\mathcal{M}_x + \mathcal{L}_y\mathcal{M}_y}{\mathcal{M}_x^2 + \mathcal{M}_y^2} \quad (\text{B.8})$$

## 345 References

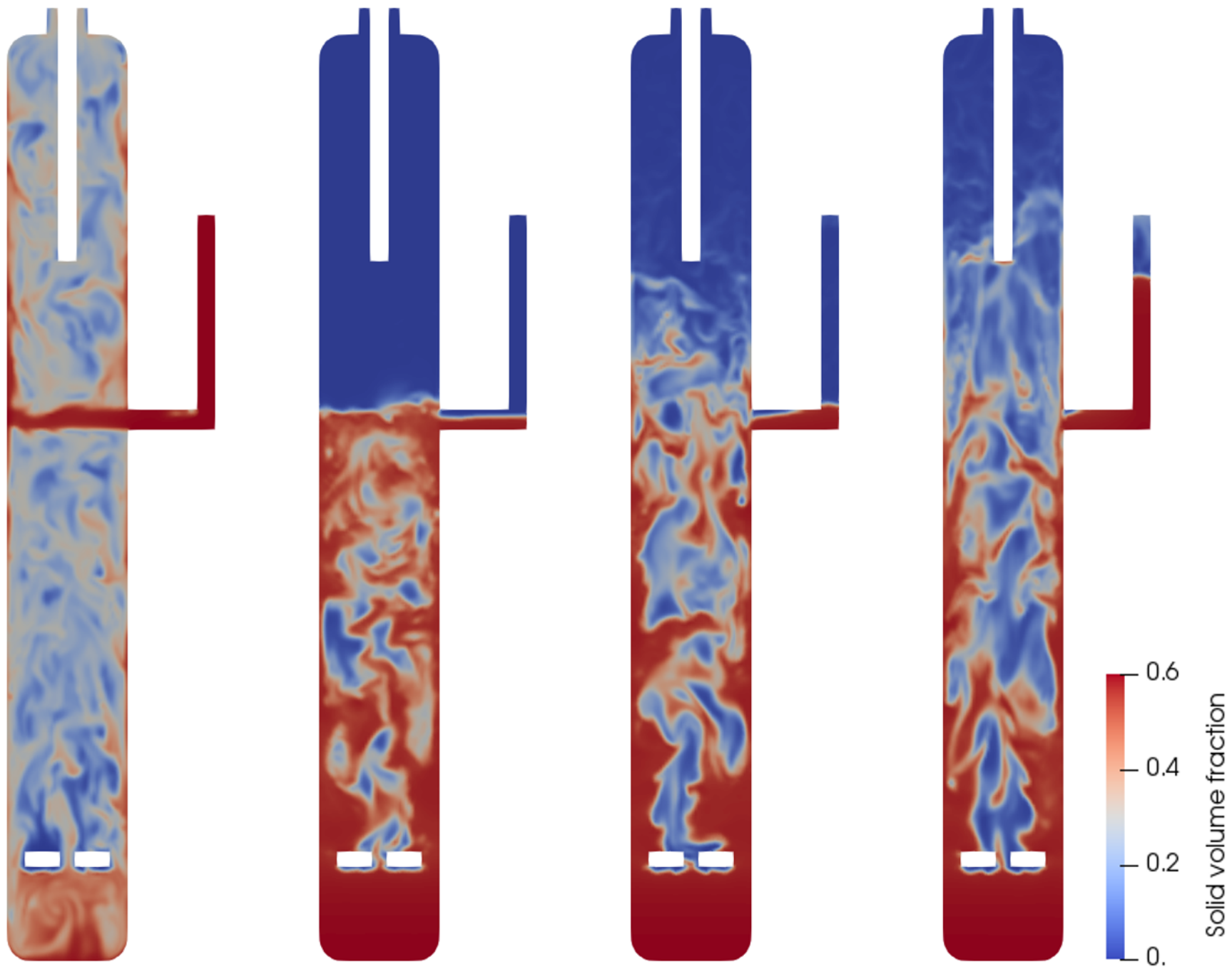
- [1] Benjamin Amblard, Raj Singh, Eusebius Gbordzoe, and Ludovic Raynal. CFD modeling of the coke combustion in an industrial FCC regenerator. *Chemical Engineering Science*, 170:731–742, 2017.
- [2] Yesim Igci and Sankaran Sundaresan. Verification of filtered two-fluid models for gas-particle flows in risers. *AIChE Journal*, 57(10):2691–2707, 2011.
- 350 [3] Jean-François Parmentier, Olivier Simonin, and Olivier Delsart. A functional subgrid drift velocity model for filtered drag prediction in dense fluidized bed. *AIChE Journal*, 58(4):1084–1098, 2012.
- [4] M.A. van der Hoef, M. van Sint Annaland, N.G. Deen, and J.A.M. Kuipers. Numerical Simulation of Dense Gas-Solid Fluidized Beds: A Multiscale Modeling Strategy. *Annual Review of Fluid Mechanics*, 40(1):47–70, 2008.
- 355 [5] Junwu Wang. A Review of Eulerian Simulation of Geldart A Particles in Gas-Fluidized Beds. *Industrial & Engineering Chemistry Research*, 48(12): 5567–5577, 2009.

- 360 [6] Simon Schneiderbauer, Stefan Puttinger, and Stefan Pirker. Comparative analysis of subgrid drag modifications for dense gas-particle flows in bubbling fluidized beds. *AIChE Journal*, 59(11):4077–4099, 2013.
- [7] William D. Fullmer and Christine M. Hrenya. The Clustering Instability in Rapid Granular and Gas-Solid Flows. *Annual Review of Fluid Mechanics*, 49(1):485–510, 2017.
- 365 [8] Jinghai Li and Mooson Kwauk. *Particle-Fluid Two-Phase Flow: The Energy-Minimization Multi-Scale Method*. Metallurgical Industry Press, Beijing, 1994.
- [9] Jinghai Li and Mooson Kwauk. Exploring complex systems in chemical engineering—the multi-scale methodology. *Chemical Engineering Science*, 58(3):521–535, 2003.
- 370 [10] Junwu Wang, Wei Ge, and Jinghai Li. Eulerian simulation of heterogeneous gas–solid flows in CFB risers: EMMS-based sub-grid scale model with a revised cluster description. *Chemical Engineering Science*, 63(6):1553–1571, 2008.
- 375 [11] Jinghai Li, Wei Ge, Jiayuan Zhang, Shiqiu Gao, Wei Wang, Ning Yang, Qicheng Sun, and Jian Gao. Analytical Multi-Scale Methodology for Fluidization Systems - Retrospect and Prospect. *The 12th International Conference on Fluidization - New Horizons in Fluidization Engineering*, 2007.
- 380 [12] Yesim Igci, Arthur T. Andrews, Sankaran Sundaresan, Sreekanth Pannala, and Thomas O’Brien. Filtered two-fluid models for fluidized gas-particle suspensions. *AIChE Journal*, 54(6):1431–1448, 2008.
- [13] A. Ozel, P. Fede, and O. Simonin. Development of filtered Euler–Euler two-phase model for circulating fluidised bed: High resolution simulation, formulation and a priori analyses. *International Journal of Multiphase Flow*, 55:43–63, 2013.
- 385

- [14] Simon Schneiderbauer. A spatially-averaged two-fluid model for dense large-scale gas-solid flows. *AIChE Journal*, 63(8):3544–3562, 2017.
- [15] Olivier Simonin. Statistical and continuum modelling of turbulent reactive particulate flows. In *Lecture Series*, volume 6, Rhode Saint Genèse, Belgium, 2000. von Karman Institute for Fluid Dynamics.
- [16] Anne Gobin, Hervé Neau, Olivier Simonin, Jean-Richard Llinas, Vince Reiling, and Jean-Lofç Sélo. Fluid dynamic numerical simulation of a gas phase polymerization reactor. *International Journal for Numerical Methods in Fluids*, 43(10-11):1199–1220, 2003.
- [17] Pascal Fede, Olivier Simonin, and Andrew Ingram. 3D numerical simulation of a lab-scale pressurized dense fluidized bed focussing on the effect of the particle-particle restitution coefficient and particle-wall boundary conditions. *Chemical Engineering Science*, 142:215–235, 2016.
- [18] Ziad Hamidouche, Enrica Masi, Pascal Fede, Renaud Ansart, Hervé Neau, Mehrdji Hemati, and Olivier Simonin. Numerical Simulation of Multiphase Reactive Flows. In *Bridging Scales in Modelling and Simulation of Non-Reacting and Reacting Flows*, volume 52, Part I, pages 55–121. Alessandro Parente Juray De Wilde, Academic Press, 1st edition, 2018.
- [19] L. Bennani, H. Neau, C. Baudry, J. Laviéville, P. Fede, and O. Simonin. Numerical simulation of unsteady dense granular flows with rotating geometries. *Chemical Engineering Research and Design*, 120:333–347, 2017.
- [20] Kapil Agrawal, Peter N. Loezos, Madhava Syamlal, and Sankaran Sundaresan. The role of meso-scale structures in rapid gas-solid flows. *Journal of Fluid Mechanics*, 445:151–185, 2001.
- [21] Arthur T. Andrews, Peter N. Loezos, and Sankaran Sundaresan. Coarse-Grid Simulation of Gas-Particle Flows in Vertical Risers. *Industrial & Engineering Chemistry Research*, 44(16):6022–6037, 2005.



- [22] Massimo Germano, Ugo Piomelli, Parviz Moin, and William H. Cabot. A  
415 dynamic subgrid-scale eddy viscosity model. *Physics of Fluids A: Fluid  
Dynamics*, 3(7):1760–1765, 1991.
- [23] D. K. Lilly. A proposed modification of the Germano subgrid-scale closure  
method. *Physics of Fluids A: Fluid Dynamics*, 4(3):633–635, 1992.



$V_f = 0.6 \text{ m/s}$   
Without SGS

$V_f = 0.3 \text{ m/s}$   
With SGS

$V_f = 0.6 \text{ m/s}$   
With SGS

$V_f = 0.85 \text{ m/s}$   
With SGS

Solid volume fraction